JOURNAL OF GEOPHYSICAL RESEARCH, VOL. 116, A07219, doi:10.1029/2011JA016476, 2011

Study of nonthermal continuum patches: Wave propagation and plasmapause study

S. Grimald,[1,2] F. El-Lemdani-Mazouz,[3] C. Foullon,[4] P. M. E. Décréau,[5] Scott A. Boardsen,[6,7] and Xavier Vallières[5]

Received 14 January 2011; revised 11 April 2011; accepted 20 April 2011; published 21 July 2011.

[1] Nonthermal continuum (NTC) radiation is believed to be emitted at the plasmapause and near the magnetic equator. We present a particular type of NTC radiation, referred to as NTC patch, which appears over a wide frequency range and within a relatively short time interval. NTC patches are observed in all magnetospheric plasma environments of the Cluster 2 orbit and are shown to represent a quarter of the NTC events observed in 2003. A statistical analysis of the frequency pattern performed on the 2003 Cluster 2 Waves of High frequency and Sounder for Probing of Electron Density by Relaxation data indicates that the NTC patches can be divided into two classes: Those with banded emission in frequency are only observed close to the source region and are thus termed "plasmaspheric," while the others, nonbanded, are termed "outer magnetospheric." In an event on 26 September 2003, we localize the sources positions and study the expected propagation of each NTC frequency beam of a plasmaspheric patch. From the observations, we show that the sources are located very close to the satellite and to each other at positions projected on the XY GSE plane. Using a ray tracing code, we demonstrate that, close to the source regions, the satellite observes all frequency rays at the same time which overlap in the spectrogram making up the plasmaspheric patch. After the satellite crossing, the rays follow diverging paths and cannot therefore be observed further out by the same satellite simultaneously. Plasmaspheric patches are thus specific signatures of close and distorted source regions.

Citation: Grimald, S., F. El-Lemdani-Mazouz, C. Foullon, P. M. E. Décréau, S. A. Boardsen, and X. Vallières (2011), Study of nonthermal continuum patches: Wave propagation and plasmapause study, *J. Geophys. Res.*, *116*, A07219, doi:10.1029/2011JA016476.

1. Introduction

[2] Nonthermal continuum (NTC) radiation is, with auroral kilometric radiation (AKR), one of the two electromagnetic emissions generated within the Earth's magnetosphere and radiated into space. NTC radiation is an incoherent narrowband electromagnetic radiation of low intensity and long duration, which is observed in a frequency range from a few 100 Hz to several 100 kHz. At low frequency, below a threshold (of order 40 kHz) function of overall magnetospheric conditions, the emission appears as broadbanded, due to multiple reflections at magnetospheric boundaries [see *Gurnett*, 1975]. NTC radiation is observed in the Earth environment [*Gurnett*, 1975; *Etcheto et al.*, 1982; *Morgan and Gurnett*, 1991; *Kasaba et al.*, 1998; *Décréau et al.*, 2004] as well as in the environment of other magnetized planets [*Kurth*, 1992]. Terrestrial NTC is widely believed to be generated at the plasmapause, a region of strong density gradient at the outer boundary of the plasmasphere [*Carpenter*, 1963; *Gringauz*, 1963], a plasma population corotating with the Earth. The primary electrostatic source has been suggested to be intense electrostatic waves, banded in frequency near values of the plasma frequency in the dawn outer plasmapause region and associated with 1–30 keV electrons [*Gurnett and Frank*, 1976]. The spacing between narrow spectral features has been related to the gyrofrequency at the source [*Gough*, 1982] using the relation

$$f = f_{UH} \sim (n + \delta) f_{ce}, \quad (1)$$

where the NTC frequency, f, the upper hybrid frequency, f_{UH}, and the electron cyclotron frequency, f_{ce}, are defined at the

[1]Centre d'Etude Spatiale des Rayonnements, Université Paul Sabatier, CNRS, Toulouse, France.
[2]Now at Institut de Recherche en Astrophysique et Planétologie, Université Paul Sabatier, CNRS, Toulouse, France.
[3]Laboratoire Atmosphère, Milieux, Observation Spatiales, CNRS, Guyancourt, France.
[4]Centre for Fusion, Space and Astrophysics, Department of Physics, University of Warwick, Coventry, UK.
[5]Laboratoire de Physique et Chimie de l'Environnement et de l'Espace, CNRS, Orléans, France.
[6]Heliophysics Science Division, NASA Goddard Space Flight Center, Greenbelt, Maryland, USA.
[7]Goddard Earth Sciences and Technology Center, University of Maryland Baltimore County, Catonsville, Maryland, USA.

0148-0227/11/2011JA016476

source; n is an integer and the quantity δ, approximated to 1/2 in an earlier publication [*Kurth et al.*, 1981], can vary between 0 and 1. There is experimental evidence that NTC sources are located near the magnetic equator [*Morgan and Gurnett*, 1991], consistent with the observations of equatorial confinement of intense f_{UH} electrostatic emissions [*Gough et al.*, 1979]. At frequencies greater than the threshold quoted above (~40 kHz), NTC emission displayed in the time-frequency spectrograms present narrowband elements. Usually, the frequency bands appear as horizontal lines as ~1 kHz frequency bandwidth and lasting several hours, although observations with 2 min period oscillatory bands have been previously reported [*Canu et al.*, 2006; *Grimald et al.*, 2009]. In the event studied by *Grimald et al.* [2009], it was shown the electrostatic wave which converts into NTC is mainly governed by the plasma density, affected by movements of the magnetic field lines.

[3] The plasmapause is approximately located at the last closed equipotential, confining the plasmasphere in the region where the corotation dominates [*Parks*, 1991; *Wolf*, 1995]. As shown by *Carpenter* [1970] and *Chappell et al.* [1970], the plasmasphere extension and the plasmapause position depend on longitude. It has also been shown that the plasmapause position changes with magnetic activity. During quiet times, the plasmapause is located at about 4 R_E in the dawn side and 7 R_E in the dusk side. During period of strong magnetic activity, the plasmapause moves inward and can be observed at a radial distance of 2 R_E. Moreover, the shape of the plasmapause changes and structures as plumes or shoulders can be observed [*Darrouzet et al.*, 2004; *Green et al.*, 2004; *Darrouzet et al.*, 2009]. If the large-scale structures of the plasmapause are quite understood, the very small ones remain unknown. The NTC sources have been shown to be of limited extent [*Etcheto et al.*, 1982; *Grimald et al.*, 2009]. This indicates that the study of NTC events can give information about the smaller scales of the plasmapause.

[4] In this paper, we present a particular NTC spectral signature which has been first observed in DE1 data [see *Olsen et al.*, 1987, Figure 1; *Jones et al.*, 1987, Figure 1; *Morgan and Gurnett*, 1991, Figure 2]. We observe it now in the Cluster data and refer to it as "patch." Contrary to the classical NTC spectral signature observed during several hours (more than 4 R_E along a given Cluster orbit) and in an about 1 kHz frequency ranges, this NTC is observed during much shorter time intervals (less than 1 h) and over large (~40 kHz) frequency ranges. Section 2 presents plasma wave observations, showing two classes of NTC patches, and a statistical study on the spatial distribution of those events along the Cluster orbit. In sections 3 and 4, we focus on one class of NTC patch and investigate its spectral signature with the study of an event observed during a Cluster perigee pass (close to the NTC source region). Section 3 discusses the source positioning and the propagation of the wave, and section 4 explores the shape and the movement of the plasmapause in the source region. Conclusions are given in section 5.

2. Wave Data

2.1. Identification of Two Classes of NTC Patches With the Cluster Constellation and WHISPER Data

[5] The Cluster mission consists of four identical satellites. They orbit in a tetrahedral configuration on a near-polar orbit with a perigee located close to the ecliptic plane at a radial distance of ≈4.5 R_E. Observations presented in this paper are derived mainly from the Waves of High frequency and Sounder for Probing of Electron density by Relaxation (WHISPER) instrument on Cluster 2 (denoted C2). The WHISPER instrument is a relaxation sounder [*Décréau et al.*, 1997, 2001] using for reception one of the two long double sphere antennas of the Electric Field and Wave (EFW) instrument [*Gustafsson et al.*, 1997]. The receiving antenna has a sphere-to-sphere separation of 88 m and rotates in the spin plane, which is parallel to the X_{GSE}-Y_{GSE} plane (where GSE refers to geocentric solar ecliptic system), at a 4 s period. The wave form is acquired and a Fast Fourier Transform (FFT) performed every 13.33 ms. Accumulated frequency spectra are delivered every 2 s [*Décréau et al.*, 2001]. Sounding operations (active mode) provide the electronic plasma frequency (f_{pe}) and the electron cyclotron frequency (f_{ce}) at a recurrence of 52 s or 104 s. Spectral signatures on natural emissions offer a better resolution (passive mode).

[6] Figure 1 presents data from the WHISPER instrument onboard Cluster 2 for two particular events observed on the 26 September 2003 (Figure 1a) and the 19 January 2003 (Figure 1b), respectively. In the first case (Figure 1a), the satellite orbits in the dipolar region, while, in the second case (Figure 1b), it travels in the lobes and in the tail. The bottom part of each panel presents a frequency-time spectrogram of electric field measured by WHISPER in its passive mode. The time intervals shown include the phenomenon of interest, i.e., NTC emissions visible above f_{pe} indicated by a solid white line. The spectrograms display similar NTC signatures visible during short times: 40 min in Figure 1a, which corresponds to a distance of 1.8 R_E along the Cluster orbit, and 25 min in Figure 1b, which corresponds to a distance of 1.1 R_E along the Cluster orbit. The frequency range of the events is about 40 kHz. Because of its large frequency range, these signatures are quite different from the classical NTC bands observed in the past with ~1 kHz frequency bandwidth. We will refer to this particular NTC signature as NTC "patches."

[7] In order to better visualize the frequency pattern of these NTC emissions, the spectrogram has been treated as follows [see also *Grimald et al.*, 2009]: each frequency spectrum has been normalized to the dynamical range covered by the spectrum (after this treatment, all spectra present intensities varying between the same two levels, minimum and maximum). Then, in each spectrum, all intensity maxima (frequency peaks) have been identified, and only those placed above a chosen intensity level have been selected. The results are displayed in the top part of each panel. In Figure 1a, a series of quasimonochromatic emissions (horizontal lines) separated by about 1.3 kHz is obtained. This result suggests that the patch is composed of several bands, with half-bandwidth comparable to their separation or overlapping in the spectrogram. In contrast, a scatter of points with no particular frequency pattern is obtained in Figure 1b. We propose that the two classes of patches identified can result from different phenomena. We next investigate their spatial distribution with respect to the source positions, located at the plasmapause and close to the equator.

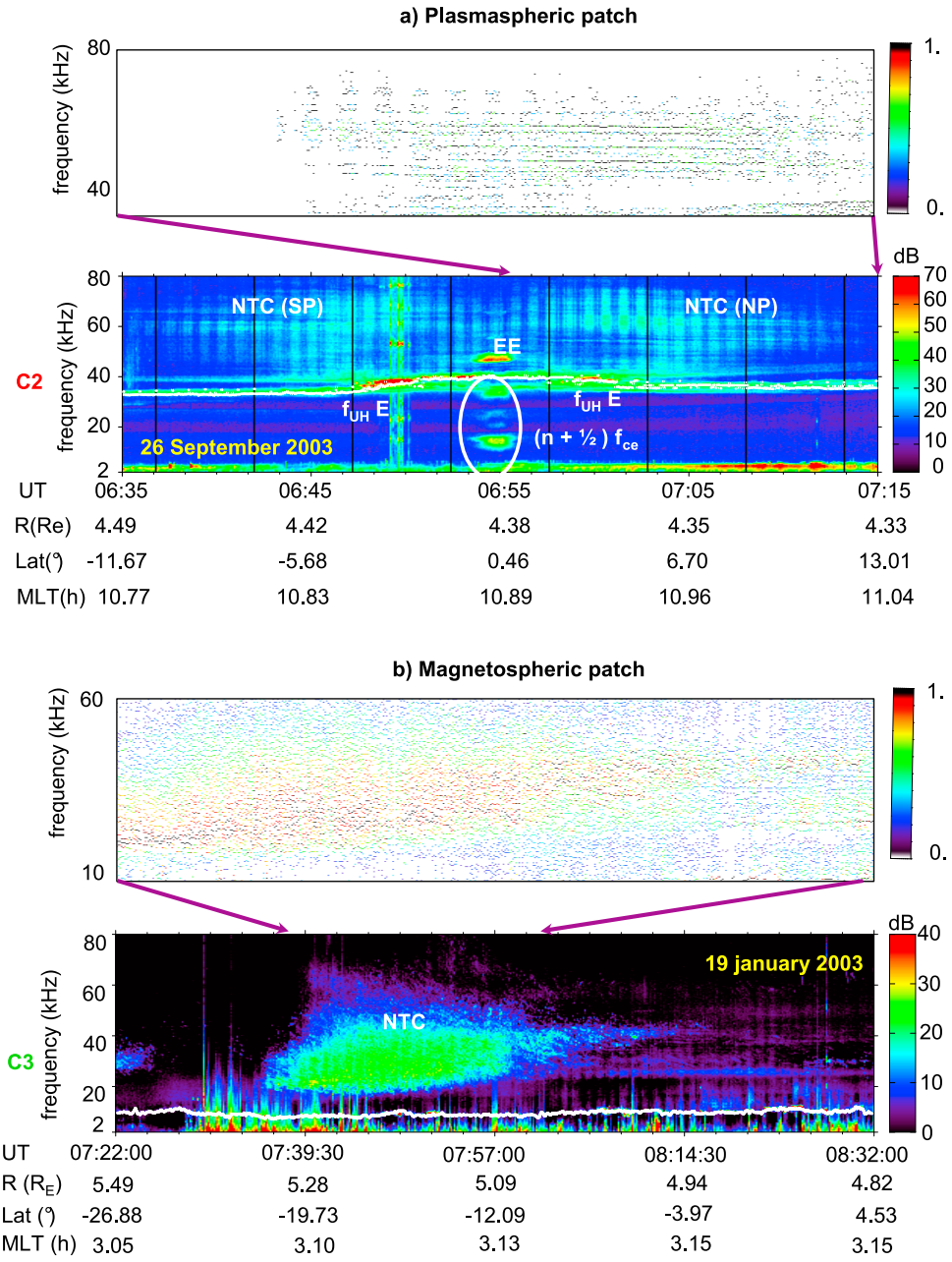

Figure 1. NTC patches observed by the WHISPER instrument on the (a) 26 September 2003 and (b) 19 January 2003 onboard C2. Positions of intensity maxima in the 40–80 kHz frequency range (lower maxima are suppressed, see text) (Figures 1a and 1b, top). In Figures Bottom of each figure: Frequency-time spectrograms of wave intensity reported in dB above 10^{-7} V_{rms} $Hz^{-1/2}$ (Figures 1a and 1b, bottom). The white line gives the local plasma frequency f_{pe}. It is noticeable that even if the spectral signatures are similar; the frequency pattern displays different structures.

2.2. Statistical Study on the Spatial Distribution of the Two Classes of Patches

[8] During the year 2003, 956 NTC events have been observed along the Cluster orbit. Those events are located inside the magnetosphere or in the solar wind. Among them, 255 (26.7%) events display patch signatures. In order to visualize the repartition of the spectral signatures in relation to the source positions, the Cluster orbit has been divided in two parts: the plasmapause region, close to the NTC source region, and all other regions including the solar wind. The events observed at the same time than the plasmapause density gradient as the 26 September 2003 event are in the first region, and the events observed when the plasmapause density gradient is not seen as the 19 January 2003 are in the second region. The diagram in Figure 2 (top) presents the distribution of the NTC signatures in the two parts of the orbit: patches with banded emission (sky blue), nonbanded

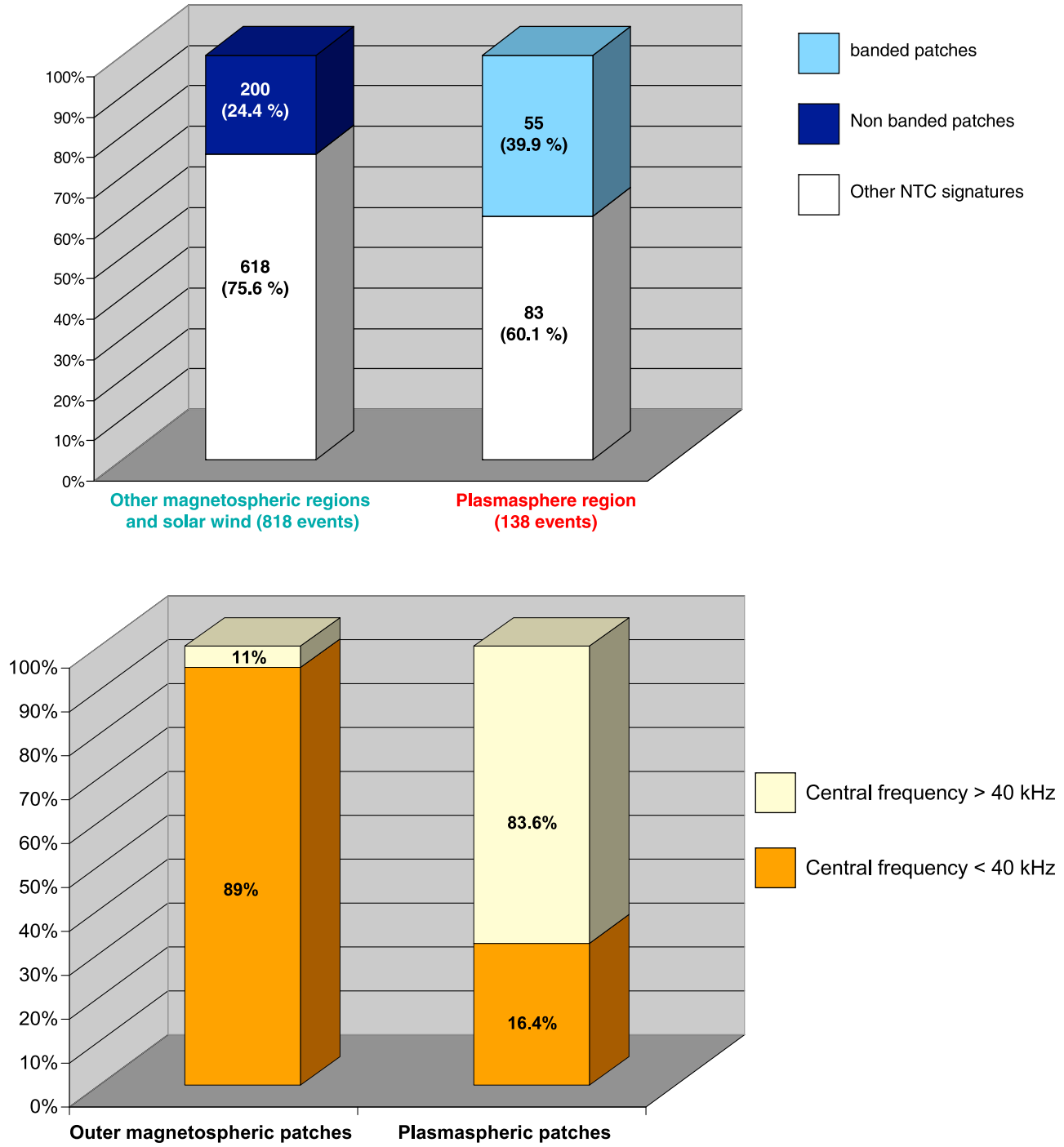

Figure 2. Statistical study on the center frequency of the patches.

patches (dark blue) and all other NTC signatures (white), i.e., classical, trapped and wide band NTC [see *Gurnett*, 1975; *Grimald et al.*, 2008]. We notice first that 39.9% of the events display the patch signature near the NTC sources while only 24.4% of the events are patches in the other magnetospheric regions and in the solar wind. Second, no nonbanded patches are observed in the plasmasphere region, when no banded patches are observed in the other magnetospheric regions and in the solar wind. In conclusion, we can differentiate between patches observed close to or far from the source regions: we will now refer to the banded patches as "plasmaspheric" patches and to the nonbanded patches as "outer magnetospheric" patches. Figure 2 (bottom) presents a bar diagram of the center frequencies of the outer magnetospheric (left bar) and plasmaspheric (right bar) patches. The bars are divided in color sections which gives the relative number of events with a center frequency above (in yellow) or below (in orange) 40 kHz. The distribution obtained shows that 89% of the outer magnetospheric patches display a center frequency below 40 kHz when only

16.4% of the plasmaspheric patches display a center frequency below this limit value. This observation confirms that the two classes of patches identified are result from different phenomena. We propose that the plasmaspheric patches disappear when the waves travel away from the source region and that the outer magnetospheric patches are made up after propagation. The nonbanded patch signature could be related to the trapped NTC and could be due to interaction of waves coming from several NTC sources located in different places in the plasmapause density gradient [*Gurnett*, 1975; *Kurth et al.*, 1981]. In section 3, we focus on the plasmaspheric patches presented in Figure 1a and perform a study of the source region and of the propagation of the waves, to understand why their frequency bands overlap in the spectrograms and why this spectral signature is not observed far from the source region.

3. Study of the Sources Positions and of the Propagation of the Wave for the 26 September 2003 Perigee Pass

3.1. Event Presentation and Sources Positions

[9] During the 26 September 2003 perigee pass, the Cluster interspacecraft separation distance is 300 km. As the spacecraft are very close, the frequency-time spectrograms of electric field measured by WHISPER onboard each satellite are similar (not shown). Coming back to the spectrogram in Figure 1a, C2 crossed the magnetic equator, at about 06:55 where localized intense electrostatic emissions are seen at frequencies $(n + 1/2)\ f_{ce}$ lying below f_{pe} (see Figure 1a). Such emissions, first observed onboard OGO 5 [*Kennel et al.*, 1970], coexist in this event with intense equatorial emissions above f_{pe} (EE in Figure 1a), close to the Bernstein frequencies f_{qs} [*Bernstein*, 1958], identified by the sounder in active mode. The latter emissions have been shown to be linked to moderate and stable magnetic activity [*El-Lemdani Mazouz et al.*, 2009]. They could be primary (electrostatic) sources of NTC, invoked in the nonlinear decay generation mechanism [*Barbosa*, 1982; *Rönnmark*, 1985]. Additional intense emissions are observed on each side of the magnetic equator, just above the plasma frequency (f_{UH} E in Figure 1a); they appear to be intensifications of a signal at the upper hybrid frequency which is present nearly continuously between 06:43 and 07:00 UT. The southern intensification occurred around 06:47 UT, and the northern intensification occurred around 06:58 UT. During the first enhancement, the receiver saturates, creating spurious replicas (roughly 10 kHz apart) of the real emission which was at about 38 kHz. These intense emissions observed near plasma frequency in the plasmapause layer on each side of the magnetic equator are the other candidates for primary sources of NTC. A detailed study of the NTC mechanism of generation is out of the scope of this paper and will be the purpose of a future work.

[10] As presented in section 2.1, the NTC emissions are seen in the frequency range 45–75 kHz during 40 min (11 520 km or 1.8 R_E). In the spectrogram in Figure 1a, two patches are observed, one on each side of the magnetic equator. Those patches are made of a series of overlapping bands whose frequency decreases slowly during the observation. They also display a periodic time variation, due to the spin modulation of the signal. Actually, the apparent period is a stroboscopic effect due to the combination of a half-spin period (2 s) with the sequencing period of instrument's operations (52 s). Assuming that this NTC radiation is electromagnetic and propagates in the O mode, the spin modulation can be used to determine the projection of the direction of propagation onto the antenna spin plane [*Calvert*, 1985; *Gurnett*, 1975; *Gough*, 1982; *Kasaba et al.*, 1998; *Décréau et al.*, 2004]. The modulation index factor m (see section 3.2), and the angle between X_{GSE} axis and raypath direction, projected onto the X_{GSE}-Y_{GSE} plane (herein referred to as ak angle) are derived from this process. The m and ak values calculated between 06:35 UT and 07:15 UT in a 30–80 kHz frequency range are presented in Figures 3a and 3b, respectively. Each propagation vector is estimated with an uncertainty factor which has been estimated of, typically, ±7° [*Décréau et al.*, 2004]. The ak angle displays a gradual evolution along the orbit (the transition from 0 to 180 degrees corresponds to a continuous transition due to sign uncertainties in the wave propagation direction), with a value about constant in all the frequency range at a given time. Therefore, the sources producing the series of narrowband elements observed in the quoted frequency range are all projected in a same source region of small extension around which the satellites travel. Occurrences of the high modulation index ($m > 73$) are visible on both sides of the equator (Figure 3a), and present a stratified structure which correspond to those peaks in the spectral power (see Figure 1a). The sources emitting the observed waves are also punctual, located close to the spin plane and are fixed or display a very low movement. Moreover, the frequency-time occurrence of a high modulation index does not correspond to any well-delimited region with specific ak angles in Figure 3b, so the source of the less modulated emissions appears to be located in the same general direction in the X_{GSE}-Y_{GSE} plane as the source of the highly modulated emission.

[11] In order to localize the source of the waves, a given frequency (61 kHz) has been chosen indicated by a white arrow in Figures 3a and 3b. When the source is punctual and can be assumed motionless, the projections onto the spin plane of the various raypaths can be used to estimate source positions by triangulation using raypaths at different times [*Morgan and Gurnett*, 1991]. Only a 2D picture of directivity in the $X_{GSE} - Y_{GSE}$ plane can be achieved from such measurements by Cluster. Figure 3c displays the orbits of C2 projected onto this plane as well as the directivity paths plotted for this satellite between 06:35 UT and 07:15 UT. The dashed line gives the projection of the magnetic equator. The directivity lines plotted at the right of the dashed lines are from the southern patch (SP) and the left ones from the northern patch (NP). It is remarkable that all the directivity lines cross in the same region, thus pointing to a single source region stable in this plane during the total time interval considered. This source region, indicated by the gray star, is small, about 0.044 R_E in diameter. We have to notice here that, the error from the uncertainty in the ak angle is contained in the diameter of the source obtained here. Because the source is very close to the satellite, despite the high value of the uncertainty on ak, the source position is obtained with a good accuracy. It is located at a distance of about 4.16 R_E from the Z_{GSE} axis, at 0.3 R_E from Cluster

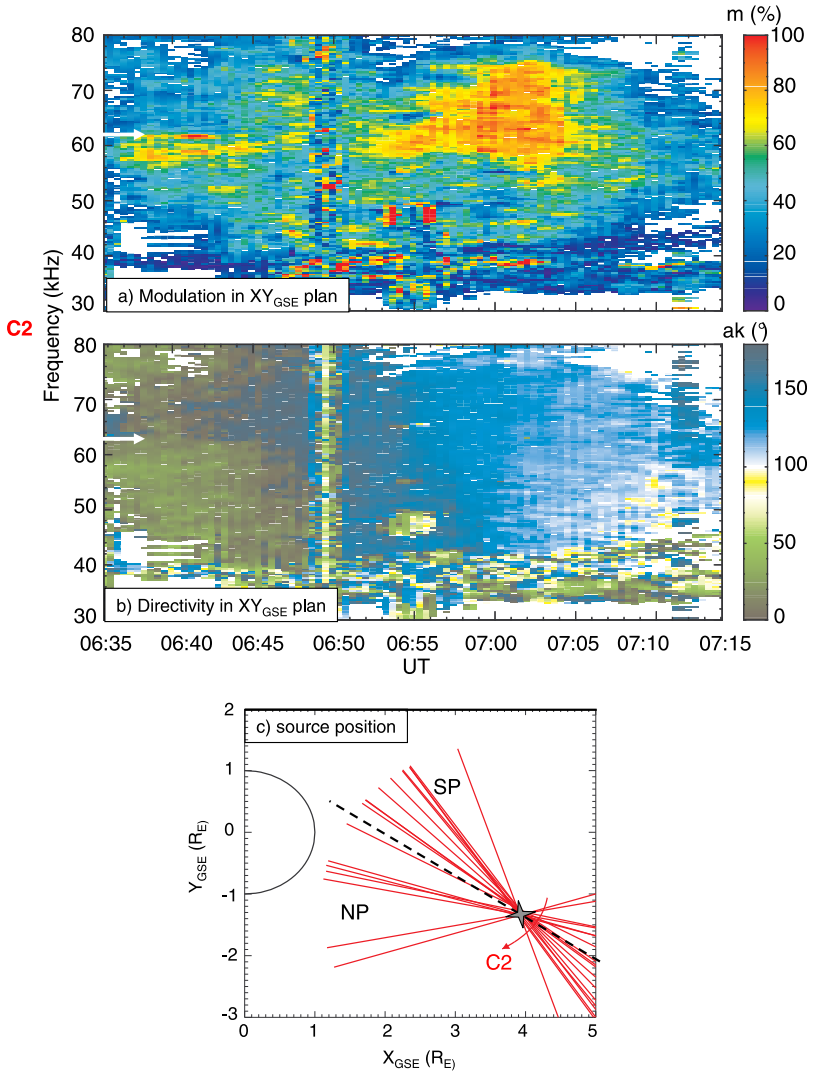

Figure 3. Parameters derived from spin modulation of electric field intensity (a) modulation index m and (b) directivity angle ak plotted as frequency-time spectrograms. (c) Triangulation in the XY GSE at 61 kHz (white arrows in Figures 3a and 3b) between 06:35 UT and 07:15 UT. Directivity lines drawn from C2 from the northern patch (NP) and the southern patch (SP) indicate a single source region (gray star) stable over the total time interval. This source intercepts the projection of the magnetic equator in the X_{GSE}-Y_{GSE} plane (black dashed line).

orbit closest approach. The small size of the source region confirms that the source region is fixed or displays a very low drift. These results suggest that the plasmapause, where the NTC sources are presumably located, is very close to the satellite position. The source position obtain using triangulation had been located using raypath from the northern and the southern patches. Figure 3a shows that two high modulation regions exist, one on each side of the equator. This suggests that the sources of the beams are different. They are very close to the magnetic equator and located at similar longitude which explains why a single source region is obtained using triangulation. It is useful to note here that an analysis of the observations for each of the other measured frequency bands yields the same result as well as an analysis of the observations for each satellite. As a consequence, we can state that the sources of the northern patch are different from the sources of the southern patch.

3.2. Model Study of the Propagation of the Waves

[12] The modulation index factor gives information about the size of the source, its movement and the orientation of the wave vector with respect to the Z_{GSE} axis. From the propagation direction analysis, we infer that the sources of the NTC radiation observed are fixed and punctual. As a consequence the variations in the modulation index factor will be due to the evolution of the angle θ between the wave vector $\vec{k}$ and the spin plane (see Figure 4). The modulation index factor used in this paper is defined as

$$m = \frac{a^2 - b^2}{a^2 + b^2} \tag{2}$$

where a is the major axis of the ellipse described by the electric field and b is the minor one. As NTC propagates in the left ordinary mode (LO mode), it displays a circular

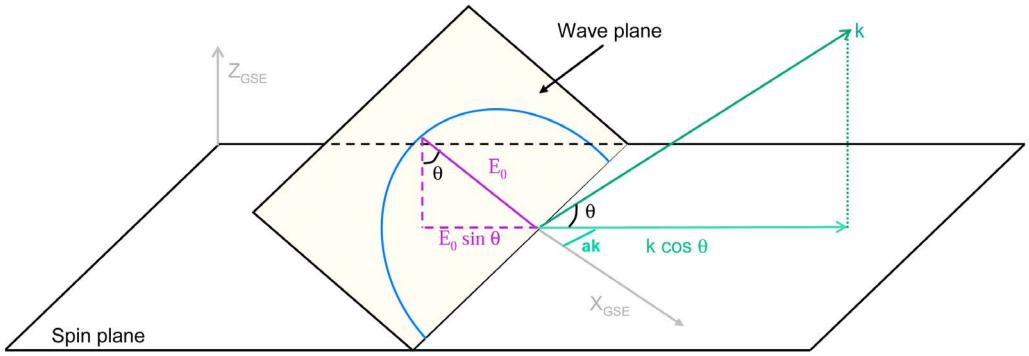

Figure 4. Geometry of a wave propagating in the O mode. The wave displays a circular polarization (in blue) in the wave plane (in yellow) which is perpendicular to the wave vector $\vec{k}$ (in green). As $\vec{k}$ is tilted by an angle of θ with the spin plane, the electric field pattern displays an elliptic polarization in this plane, with a major axis a = E_0 and a minor axis b = E_0 sin θ.

polarization in the wave plane. If $\vec{k}$ is tilted by an angle of θ to the spin plane, then the polarization pattern in this plane is an ellipse with a = E_0 and b = E_0 sin θ (see Figure 4), where E_0 is the electric field amplitude. As a consequence, relation (2) can be rewritten as

$$m = \frac{1 - \sin^2 \theta}{1 + \sin^2 \theta}, \tag{3}$$

and the θ angle can be calculated using the relation:

$$\theta = \frac{1}{2} \arccos \frac{3m - 1}{m + 1} \tag{4}$$

From the θ and the ak angle, it is possible to determine the direction of the wave vector in 3D. We notice here that, using relation (4), two values of θ are obtained. In each example, the θ angle directing the path away from the magnetic equator has been chosen. For this event, the θ angle is estimated with an uncertainty of ±3°.

[13] Using the wave vector it is possible to calculate the path followed by the wave after its observation by the satellite. To determine the raypath at different frequencies during the 26 September 2003 event, the ray tracing code developed by *Green* [1988] has been used. As NTC propagates without interaction with the magnetic field (f > fpe ≫ fce) from the source position, the magnetic field model in the simulation is a dipolar one. The plasma density model is a combination of several models (diffusive equilibrium model by *Angerami and Thomas* [1964], plasmasphere model by *Kimura* [1966], plasmapause by *Aikyo and Ondoh* [1971], and magnetopause by *Roelof and Sibeck* [1993]). The final model is Kp dependant, which accounts for changes in the plasmaspause due to magnetic activity. In order to model a plasmapause with a density profile similar to the one observed in the WHISPER data (see Figure 1a), a Kp = 4.3 has been used. Figure 5 presents the results obtained using C2 position at 06:40 UT (Figure 5a) and 07:00 UT (Figure 5b) as a starting point. The raypaths for wave propagating at 54.4 kHz (dark blue), 60.1 kHz (red), 70 kHz (green) and 75 kHz (light blue) are shown. In Figure 5, the satellite position is given by the red triangle. For each example, the rays propagate in the day side, away from the Earth and the magnetic equator (gray line in Figure 5 (right)). At a given time, they propagate in the same general direction, which is different from 06:40 UT to 07:00 UT: the raypaths make their way toward the dusk sector in Figure 5a, while they make it toward dawn in Figure 5b (left). For each example, the rays propagate straight until the magnetopause. It is important to notice here that each ray follows its own path, propagating separately. Moreover, when the ray intercepts the magnetopause, two behaviors are observed. First, at 60.1 kHz, 70 kHz and 75 kHz the rays propagate at a frequency greater than the magnetopause f_{pe}. As a consequence, they cross the magnetopause to propagate freely in the solar wind. Due to the increasing density at the magnetopause crossing, they are slightly deflected (violet arrows in Figure 5), the change in direction being more or less important, depending on the difference between the frequency of the wave and the local plasma frequency. Second, the ray at 54.4 kHz propagates at a frequency smaller than the magnetopause f_{pe}. As a consequence it bounces at the magnetopause boundary and is reflected inside the magnetosphere. This phenomenon happens each time the ray encounters the magnetopause (brown arrows). This will again increase the distance between each raypaths. As a consequence, a satellite traveling away from the source region may encounter only a part of the ray beams and it will encounter them one after another. This would explain why the banded patches are not observed further out in the magnetosphere.

4. Study of the Plasmasphere and of the Sources Region

4.1. Geomagnetic Conditions and Plasmapause Shape in the Source Region

[14] We focus now on the shape of the part of the plasmapause in the source region. The satellites travel from the Southern Hemisphere to the Northern Hemisphere (see Figure 1a) at about 11 h MLT. During the perigee pass, f_{pe} increases and decreases spanning a range of frequencies between 33 and 42 kHz indicating a plasmapause approach (see Figure 1a). However, the smooth variation of the plasma frequency shows that the spacecraft only intercepts

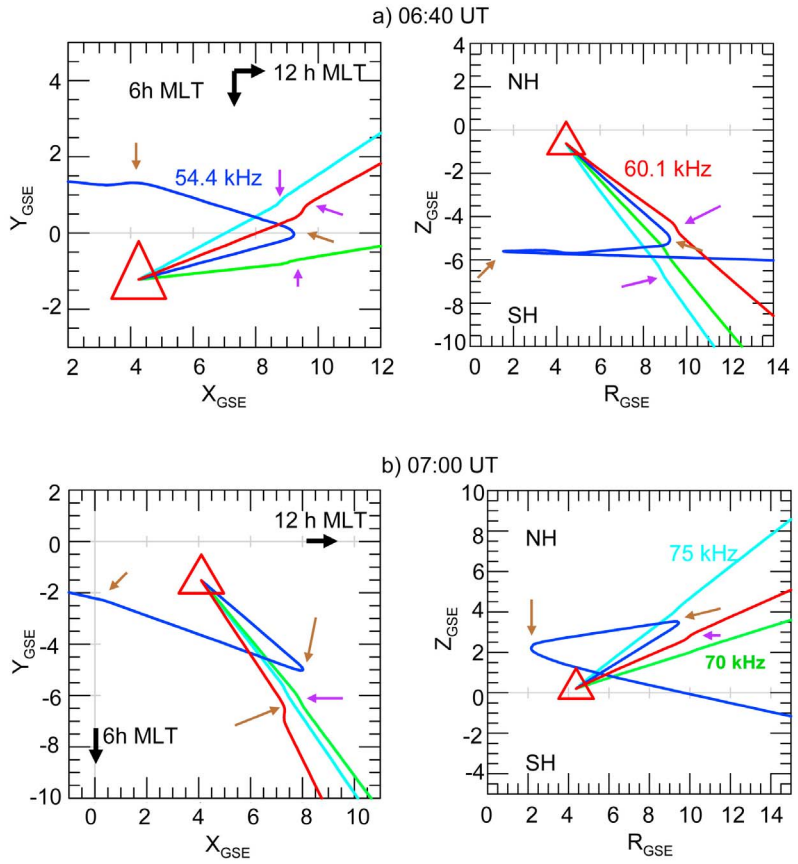

Figure 5. Ray tracing at 54.4 kHz (dark blue), 60.1 kHz (red), 70 kHz (green), and 75 kHz (light blue) at (a) 06:40 UT and (b) 07:00 UT. In each plot, the brown arrows indicate bounce at the magnetopause boundary, and the violet arrows indicate deflection of the raypaths due to the magnetopause encounter.

the outer plasmasphere, as the main plasmasphere body appears to have been compressed to L values below Cluster orbits. During the perigee pass under study, the Kp index is low (Kp = 2.7). This normally indicates the plasmapause to be far from Earth (see *Pierrard and Lemaire* [2004] for a link between the plasmapause position and the Kp index). However, we can notice an increase of the Kp index up to 6 on 24 September 2003, which stay above 4 during two days and decrease at the beginning of 26 September. Moreover, the Dst index indicates two moderate magnetic storms (-50 nT $\leq$ Dst ≤ -100 nT, see *Loewe and Prölss* [1997]) occurring on 24 and 25 September 2003 linked with an increase of the auroral electrojet activity (600 nT < AE < 1100 nT). The AU index (210 nT < AU < 360 nT) shows a small compression of the dayside magnetopause, while the AL index (-950 nT < AL < -550 nT) indicates an injection of particles coming from the night side. To summarize these observations, there were two magnetic storms responsible for a small increase of the ring current activity and for an injection of particles in the auroral region in the days before the perigee pass. In conclusion, the earlier active geomagnetic conditions have affected the plasmapause, such that it has been likely compressed to low L values and that its position, below Cluster perigee, cannot be evaluated accurately by direct observation. Nevertheless, as the NTC sources are located in the plasmapause density gradient, it is evident from the study presented in section 3.1 that the plasmapause is very close from the satellite position. Moreover, the NTC sources are localized in the plasmapause density gradient, in a region where f_{UH} is approximately the electron plasma frequency. Using triangulation, it is possible to determine the source position for several frequencies [*Décréau et al.*, 2004]. Assuming that the sources of NTC are located at a position where $f_{NTC} = f_{UH}$, it is possible to determine the density profile of the plasmapause in the source region (see also first attempt and different approach by *Grimald et al.* [2009]). The result obtained is presented in Figure 6. As discussed above (section 3.1) the sources of the northern patch are different from the sources of the southern patch. The first ones are located in the Northern Hemisphere when the second ones are in the Southern Hemisphere. As a consequence, the study has been performed for each patch and the density profiles obtained at 06:40 UT (Southern patch, Figure 6a) and at 07:00 UT (Northern patch, Figure 6b) are represented. For each case, the source position has been determined using triangulation at different frequencies and located in Figure 6 using black crosses. Only the frequencies giving well define source positions have been represented. The black horizontal lines give the error bar for each source position. Thus, the overall

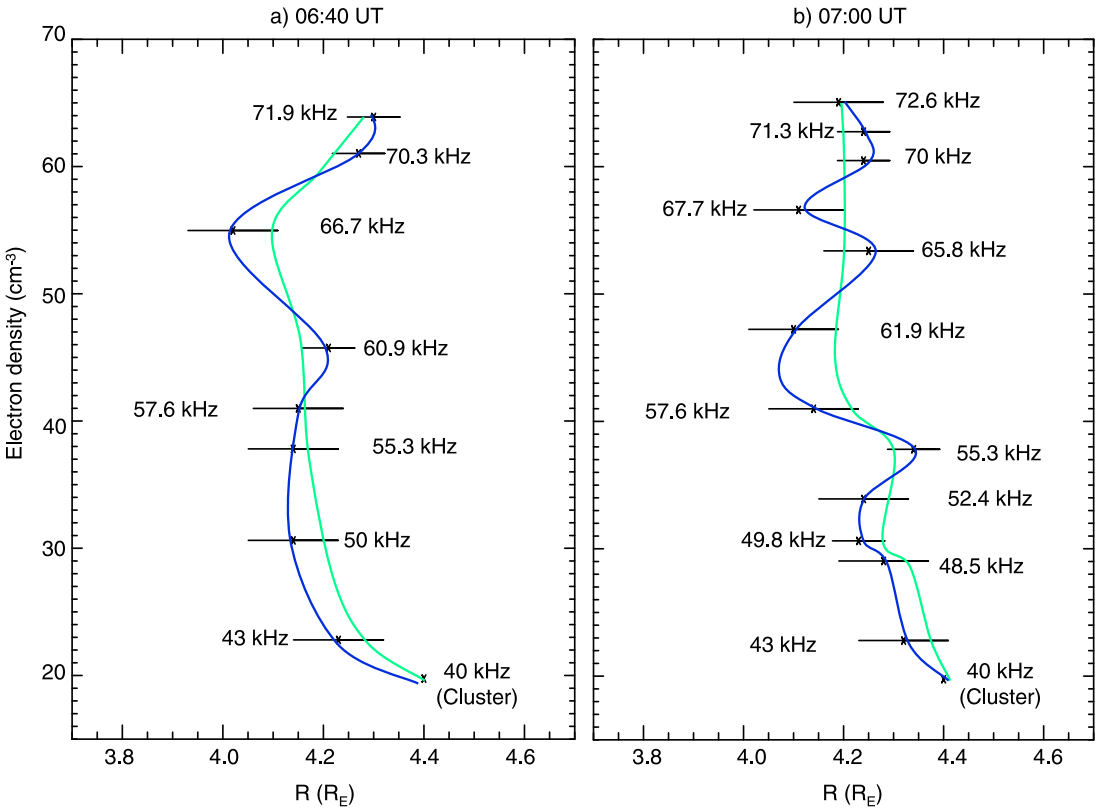

Figure 6. Electron number density profile of the plasmapause projected in the spin plane versus radial R near the Cluster spacecraft at (a) 06:40 UT and (b) 07:00 UT. The sources' positions obtained using triangulation are indicated by the black crosses and the error bars are associated (black lines). Two examples of plausible density profiles (blue and green lines) are shown for each time.

sources' region obtained is of relatively small radial extent (~0.5 R_E), which is in agreement with previous observation made by *Grimald et al.* [2009]. The sources are located in a very strong density gradient ($\Delta n_e = 44$ cm^{-3} over a distance of 0.5 R_E). We have to note that the sources are located at different longitude and at different latitude. The observations show that, for each patch, the sources are located in a 13 min MLT range. They are not at the same position, just at the same geocentric distances. The green and the blue lines in Figure 6 give two examples of plausible density profiles for each time. It is evident that small scales structures exist in the plasmasphere surface: each profile display undulations with radial amplitude of at most 0.5 R_E. To summarize, the plasmapause has been eroded and distorted by earlier magnetic activity such as it is located at about 4.2 R_E. The part of the plasmapause containing the source region is very close to the satellite position and display a very strong density gradient with structures which may be involved in the NTC generation mechanism. We have to note here that at 4.2 R_E, $f_{ce\ source} \approx 12$ kHz. From equation (1), the sources may emit waves at $f = (n + 1/2)\ f_{ce}$ and the difference in frequency Δf between two bands may be $f_{ce\ source}$, which is very different from the 1.3 kHz observed in Figure 1a. The source localization highlights the proximity of the sources inside the density gradient. As a consequence, the frequencies of the beams emitted are very similar which explain the overlapping of the bands in the spectrogram.

4.2. Study of the Plasmapause Movement

[15] Figure 7a presents the magnetic field amplitude measured by the Fluxgate Magnetometer (FGM) instrument [*Balogh et al.*, 2001] onboard C2 (B_{FGM}, in blue) and a modeled magnetic field [*Tsyganenko and Stern*, 1996] ($B_{Tsyganenko}$, in orange). The magnetic field measured by the satellite is higher than the modeled one, indicating a change in the current intensity in the region crossed by C2. As presented in section 4.1, the Dst index indicates two moderate magnetic storms occurring on 24 and 25 September 2003. This may be responsible for the change in the current intensity in the inner magnetosphere and for a decreasing magnetic field. A more detailed observation shows that some oscillations appear in the B_{FGM} evolution (black arrows) which is not seen in the modeled magnetic field. In order to highlight these oscillations, the modeled magnetic field has been subtracted from the measured magnetic field. The result is presented in Figure 7b. The oscillations observed have period P = 5 min 13 s indicating ULF pulsations in the Pc5 pulsations frequency range (1–10 mHz). They have small amplitude (a few nT), are observed in all the magnetic field components and in phase between the four Cluster satellites (not shown). As shown by *Grimald et al.* [2009], those oscillations may be reflected in the NTC bands. They may be some oscillations in the NTC bands on the 26 September 2003 event as well, but those are not well resolved because of their very small amplitude and

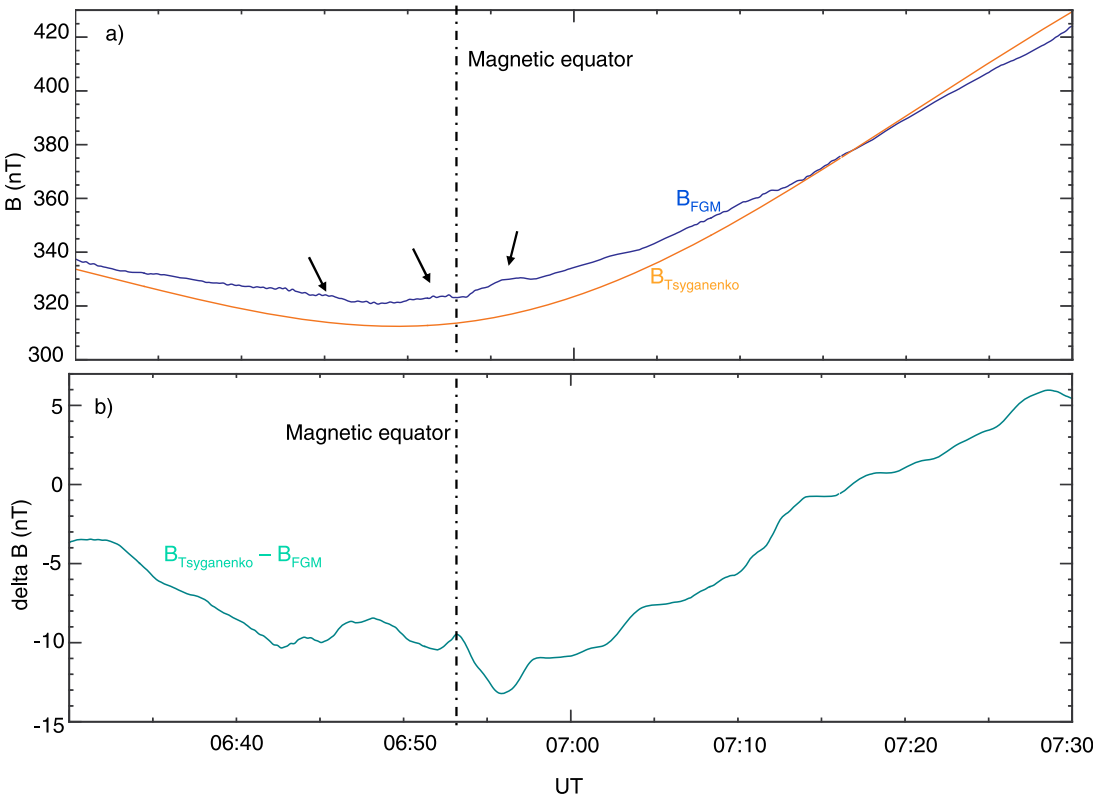

Figure 7. (a) Magnetic field amplitude measured by the FGM instrument onboard Cluster 2 (blue line) and modeled magnetic field (orange line). The black arrows indicate oscillations in the magnetic field amplitude. (b) Qualitative variations of the magnetic field amplitude. In each plot, the magnetic equator is indicated by a black dash-dotted line.

the much larger period of the magnetic field oscillations. Those oscillations generate small amplitude oscillations in the plasma density which are in turn reflected in the NTC bands but with an amplitude of the NTC band oscillations below the resolution of the WHISPER instrument.

[16] The bands observed in the top of Figure 1a are parallel and separated by about 1.3 kHz. Between 07:00 and 07:15 UT, the bands decrease slowly with time by about 12 kHz.min^{-1}. As $f_{NTC} = f_{UH} \approx f_{pe}$, this observation leads to the conclusion that the density at the source position decreases by about 2×10^{-4}cm^{-3}.min^{-1}. Assuming the source does not move, the position of maximum density gradient is moving inward. It has been shown that $\Delta n_e = 44$ cm^{-3} over a distance of 0.5 R_E. This leads to the conclusion that the surface moves earthward very slowly, with a velocity $V \approx 0.24$ m.s^{-1}. The question now is to determine whether the whole plasmasphere is moving or if it is only the source region. One possibility is that the surface drift velocity results from the ULF oscillation radial amplitude, corresponding to radial scale sizes of the order of ($V \times P/2 =$) 38 m. This scale size is much smaller than the size of the sources' region or even the changes in average plasmapause locations between Figures 6a and 6b. Thus the spatial inhomogeneties of the plasmaspheric surface are not caused by the ULF waves.

[17] Prior to the surface drift, an increase of the interplanetary magnetic field (IMF) and of the solar wind velocity is observed near the bow shock from about 06:53 UT to 07:03 UT (not shown). This is well known to increase the convection electric field inside the magnetosphere [*Burton et al.*, 1975; *Dungey*, 1961]. The Alfvén boundary layer is defined as the position where the convection electric field is equal to the corotation one [*Alfvén*, 1968; *Volland*, 1973; *Stern*, 1975]. The plasmasphere is located in the part of the magnetosphere where the corotation dominates. An increasing of the convection electric field is responsible for an inward movement of the Alfvén boundary layer. As a consequence, the plasmasphere is less extended and the plasmapause moves inward. This is in agreement with the observations made on the NTC bands, but also shows that it is not only the source region which is moving inward, but the whole plasmapause.

5. Discussion and Conclusion

[18] We have presented an original NTC spectral signature, termed NTC patch, which contrary to the classical NTC, is displayed over a large frequency band (~40 kHz) and relatively short time interval (40 min). Two different patch events have been described: the first one displays a banded structure, while the second one displays no frequency pattern. In the first instance, a statistical study performed on the 2003 Cluster 2 WHISPER data set highlights that the banded patches are only observed close to the source region, while the nonbanded ones are observed everywhere else in the orbit. This observation allows

dividing the patches in two classes: the plasmaspheric patches, or banded ones, and the outer magnetospheric patches, or non banded ones. We propose that the nonbanded patch signature could be related to the trapped NTC and could be due to interaction of waves coming from several NTC sources located in different places in the plasmapause density gradient [*Gurnett*, 1975; *Kurth et al.*, 1981]. NTC emissions are linked with injection of energetic particles in the plasmasphere [*Gough*, 1982]. Because of the low magnetic activity just before and during the observation, few sources may be active in the plasmapause density gradient. Because of the magnetopause shape, a convergence of trapped NTC beams is observed but not enough beams travel inside the magnetosphere to make the long lasting signature of the trapped NTC as defined by *Gurnett* [1975].

[19] In the second instance, we have analyzed the plasmaspheric patch event observed during the 26 September 2003 perigee pass. In this event, patches are observed on each side of the magnetic equator. The analysis of the spectral signature shows that the large frequency range comes from a series of narrowbands observed at the same time with very close frequency. As a consequence, those bands overlap in the spectrogram. The data analysis provides here the NTC source localization, a model study of the propagation of the wave further out in the magnetosphere and a study of the shape and movement of the emitting surface. It has been shown that the NTC emission in all frequency bands comes from a small source region located not far from the satellites' orbits when the spacecraft cross the magnetic equator. Each patch has its own sources, distributed around the magnetic equator. Each source emits a beam of wave at a frequency $f_{NTC} \approx f_{pe\ source}$, where $f_{pe\ source}$ is the electron plasma frequency at the source position, which propagates alone and follows its own path. As the spacecraft is very close to the source position, it observes all beams at the same time and they overlap in the spectrograms. Far from the source position, the beams are separated and cannot be observed together. This is why there are no banded patches observed far from the source region. The study of the source position also allows a quantitative test of equation (1) by comparing the sources positions obtained using triangulation and the f_{ce} value in the source region. From the number of sources obtained in a gyroharmonic band, we infer that the electrostatic wave, which converts into NTC may not be linked to f_{ce}. Some mechanisms implying the Bernstein modes were developed by *Oya* [1971], *Melrose* [1981], *Christiansen et al.* [1984], and *Rönnmark* [1985]. Those mechanisms seem to be more relevant here (as given by *Grimald et al.* [2009]) but remain to be tested. Furthermore, we demonstrate that a study of the source position and of the evolution in frequency of the NTC band can be used to study the plasmapause and the plasmasphere themselves. The results show that the plasmasphere has been compressed by earlier magnetic activity and is moving inward. The plasmapause is distorted and presents very strong density gradients which may be involved in the NTC generation mechanism.

[20] **Acknowledgments.** S.G. and F. E. acknowledge financial support from the Centre National des Etudes Spatiales (CNES). C.F. acknowledges financial support from the UK Science and Technology Facilities Council (STFC) on the CFSA Rolling Grant. We would like to thank the WEC, JSOC, and ESOC teams for continuous support of Cluster operations. S.G., F.E., and C.F. thank P. Décréau, J. G. Trotignon and the WHISPER team, E. Lucek and the FGM team. Data analysis was done with the QSAS science analysis system provided by the UK Cluster Science Centre (Imperial College London and Queen Mary, University of London) supported by STFC.

[21] Robert Lysak thanks the reviewers for their assistance in evaluating this paper.

References

Aikyo, K., and T. Ondoh (1971), Propagation of nonducted VLF waves in the vicinity of the plasmapause, *J. Radio Res. Lab. Jpn.*, *18*, 153.

Alfvén, H. (1968), Some properties of magnetospheric neutral surfaces, *J. Geophys. Res.*, *73*, 4379, doi:10.1029/JA073i013p04379.

Angerami, J., and J. Thomas (1964), The distribution of ions and electrons in the Earth's exosphere, *J. Geophys. Res.*, *69*, 4537, doi:10.1029/JZ069i021p04537.

Balogh, A., et al. (2001), The Cluster magnetic field investigation: Overview of in-flight performance and initial results, *Ann. Geophys.*, *19*, 1207, doi:10.5194/angeo-19-1207-2001.

Barbosa, D. D. (1982), Low-level VLF and LF radio emissions observed at Earth and Jupiter, *Rev. Geophys.*, *20*, 316, doi:10.1029/RG020i002p00316.

Bernstein, I. B. (1958), Waves in a plasma in a magnetic field, *Phys. Rev.*, *109*, 10, doi:10.1103/PhysRev.109.10.

Burton, R. K., R. L. Mc Pherron, and C. T. Russel (1975), An empirical relationship between interplanetary conditions and Dst, *J. Geophys. Res.*, *80*, 4204, doi:10.1029/JA080i031p04204.

Calvert, W. (1985), DE-1 measurements of AKR wave directions, *Geophys. Res. Lett.*, *12*, 381, doi:10.1029/GL012i006p00381.

Canu, P., P. Décréau, S. Escoffier, and S. Grimald (2006), Observations of continuum radiation close to the plasmapause: Evidence for small scale sources, in *Planetary Radio Emissions VI: Proceedings of the 6th International Workshop Held at Graz, Austria April 20–22, 2005*, edited by H. O. Rucker, W. S. Kurth, and G. Mann, pp. 289–297, Akademie, Vienna.

Carpenter, D. L. (1963), Whistler evidence of a "knee" in the magnetospheric ionization density profile, *J. Geophys. Res.*, *68*, 1675, doi:10.1029/JZ068i006p01675.

Carpenter, D. L. (1970), Whistler evidence of the dynamic behavior of the duskside bulge in the plasmasphere, *J. Geophys. Res.*, *75*, 3837, doi:10.1029/JA075i019p03837.

Chappell, C. R., K. K. Harris, and G. W. Sharp (1970), A study of the influence of magnetic activity on the location of the plasmapause as measured by OGO 5, *J. Geophys. Res.*, *75*, 50, doi:10.1029/JA075i001p00050.

Christiansen, P. J., J. Etcheto, K. Ronmark, and L. Stenflo (1984), Upper hybrid turbulence as a source of nonthermal continuum radiation, *Geophys. Res. Lett.*, *11*, 139, doi:10.1029/GL011i002p00139.

Darrouzet, F., et al. (2004), Density structures inside the plasmasphere: Cluster observations, *Ann. Geophys.*, *22*, 2577, doi:10.5194/angeo-22-2577-2004.

Darrouzet, F., et al. (2009), Plasmaspheric density structures and dynamics: Properties observed by the CLUSTER and IMAGE missions, *Space Sci. Rev.*, *145*, 55, doi:10.1007/s11214-008-9438-9

Décréau, P. M. E., et al. (1997), WHISPER, a resonance sounder and wave analyser: Performances and perspectives for the Cluster mission, *Space Sci. Rev.*, *79*, 157, doi:10.1023/A:1004931326404.

Décréau, P. M. E., et al. (2001), Early results from Whisper instrument on Cluster: An overview, *Ann. Geophys.*, *19*, 1241, doi:10.5194/angeo-19-1241-2001.

Décréau, P. M. E., et al. (2004), Observation of Continuum radiations from the CLUSTER fleet: First results from direction finding, *Ann. Geophys.*, *22*, 2607, doi:10.5194/angeo-22-2607-2004.

Dungey, J. W. (1961), Interplanetary magnetic field and the auroral zones, *Phys. Rev. Lett.*, *6*, 47, doi:10.1103/PhysRevLett.6.47.

El-Lemdani Mazouz, F., J. L. Rauch, P. M. E. Décréau, J. G. Trotignon, X. Vallières, F. Darrouzet, P. Canu, and X. Suraud (2009), Wave emissions at half electron gyroharmonics in the equatorial plasmasphere region: CLUSTER observations and statistics, *Adv. Space Res.*, *43*, 253, doi:10.1016/j.asr.2008.06.007.

Etcheto, J., P. J. Christiansen, M. P. Gough, and J. G. Trotignon (1982), Terrestrial continuum radiation observations with GEOS-1 and ISEE-1, *Geophys. Res. Lett.*, *9*, 1239, doi:10.1029/GL009i011p01239.

Gough, M. P. (1982), Nonthermal continuum emissions associated with electron injections: Remote plasmapause sounding, *Planet. Space Sci.*, *30*, 657, doi:10.1016/0032-0633(82)90026-5.

Gough, M. P., P. J. Christiansen, G. Martelli, and E. J. Gershuny (1979), Interaction of electrostatic waves with warm electrons at the geomagnetic equator, *Nature*, *279*, 515, doi:10.1038/279515a0.

Green, J. L. (1988), Ray tracing planetary radio emissions, in *Planetary Radio Emissions II: Proceedings of 2nd International Workshop Held at Graz, Austria, September 7–9, 1987*, edited by H. O. Rucker, S. J. Bauer, and B. M. Pedersen, pp. 355–379, Akademie, Vienna.

Green, J. L., S. Boardsen, S. F. Fung, H. Matsumoto, K. Hashimoto, R. R. Anderson, B. R. Sandel, and B. W. Reinisch (2004), Association of kilometric continuum radiation with plasmaspheric structures, *J. Geophys. Res.*, *109*, A03203, doi:10.1029/2003JA010093.

Grimald, S., P. M. E. Décréau, P. Canu, A. Rochel, and X. Vallières (2008), Medium latitude sources of plasmaspheric nonthermal continuum radiations observed close to harmonics of the electron gyrofrequency, *J. Geophys. Res.*, *113*, A11216, doi:10.1029/2008JA013290.

Grimald, S., C. Foullon, P. M. E. Décréau, G. Le Rouzic, X. Suraud, and X. Vallières (2009), Modulation of NTC frequencies by Pc5 ULF pulsations: Experimental test of the generation mechanism and magnetoseismology of the emitting surface, *J. Geophys. Res.*, *114*, A11211, doi:10.1029/2009JA014270.

Gringauz, K. I. (1963), The structure of the ionized gas envelope of Earth from direct measurements in the U.S.S.R. of local charged particle concentrations, *Planet. Space Sci.*, *11*, 281, doi:10.1016/0032-0633(63)90030-8.

Gurnett, D. A. (1975), The Earth as a radio source: The nonthermal continuum, *J. Geophys. Res.*, *80*, 2751, doi:10.1029/JA080i019p02751.

Gurnett, D. A., and L. A. Frank (1976), Continuum radiation associated with low-energy electrons in the outer radiation zone, *J. Geophys. Res.*, *81*, 3875, doi:10.1029/JA081i022p03875.

Gustafsson, G., et al. (1997), The electric field and wave experiment for the Cluster mission, *Space Sci. Rev.*, *79*, 137, doi:10.1023/A:1004975108657.

Jones, D., W. Calvert, D. A. Gurnett, and R. L. Huff (1987), Observed beaming of terrestrial myriametric radiation, *Nature*, *328*, 391, doi:10.1038/328391a0.

Kasaba, Y., et al. (1998), Remote sensing of the plasmapause during substorms: Geotail observation of nonthermal continuum enhancement, *J. Geophys. Res.*, *103*, 20,389, doi:10.1029/98JA00809.

Kennel, C. F., et al. (1970), VLF electric field observations in the magnetosphere, *J. Geophys. Res.*, *75*, 6136, doi:10.1029/JA075i031p06136.

Kimura, I. (1966), Effects of ions on whistler mode ray tracing, *Radio Sci.*, *1*, 269.

Kurth, W. S. (1992), Continuum radiation in planetary magnetospheres, in *Planetary Radio Emission III: Proceedings of 3rd International Workshop Held at Graz, Austria, September 2–4, 1991*, edited by H. O. Rucker, S. J. Bauer, and M. L. Kaiser, pp. 329–350, Akademie, Vienna.

Kurth, W. S., D. A. Gurnett, and R. R. Anderson (1981), Escaping nonthermal continuum radiation, *J. Geophys. Res.*, *86*, 5519, doi:10.1029/JA086iA07p05519.

Loewe, C. A., and G. W. Prölss (1997), Classification and mean behavior of magnetic storms, *J. Geophys. Res.*, *102*, 14,209, doi:10.1029/96JA04020.

Melrose, D. B. (1981), A theory of nonthermal continua in the terrestrial and Jovian magnetospheres, *J. Geophys. Res.*, *86*, 30, doi:10.1029/JA086iA01p00030.

Morgan, D. D., and D. A. Gurnett (1991), The source location and beaming of terrestrial continuum radiation, *J. Geophys. Res.*, *96*, 9595, doi:10.1029/91JA00314.

Olsen, R. C., S. D. Shawhan, D. L. Gallagher, J. L. Green, C. R. Chappell, and R. R. Anderson (1987), Plasma observations at the Earth's magnetic equator, *J. Geophys. Res.*, *92*, 2385, doi:10.1029/JA092iA03p02385.

Oya, H. (1971), Conversion of electrostatic plasma wave into electromagnetic waves: Numerical calculation of the dispersion relation for all wavelengths, *Radio Sci.*, *6*, 1131, doi:10.1029/RS006i012p01131.

Parks, G. K. (1991), *Physics of Space Plasmas: An Introduction*, Addison-Wesley, Redwood City, Calif.

Pierrard, V., and J. F. Lemaire (2004), Development of shoulders and plumes in the frame of the interchange instability mechanism for plasmapause formation, *Geophys. Res. Lett.*, *31*, L05809, doi:10.1029/2003GL018919.

Roelof, E. C., and D. G. Sibeck (1993), Magnetopause shape as a bivariate function of interplanetary magnetic field B_z and solar wind dynamic pressure, *J. Geophys. Res.*, *98*, 21,421, doi:10.1029/93JA02362.

Rönnmark, K. (1985), Generation of magnetospheric radiation by decay of Bernstein waves, *Geophys. Res. Lett.*, *12*, 639, doi:10.1029/GL012i010p00639.

Stern, D. P. (1975), The motion of a proton in the equatorial magnetosphere, *J. Geophys. Res.*, *80*, 595, doi:10.1029/JA080i004p00595.

Tsyganenko, N. A., and D. P. Stern (1996), Modeling the global magnetic field of the large-scale Birkeland current systems, *J. Geophys. Res.*, *101*, 27,187, doi:10.1029/96JA02735.

Volland, H. (1973), A semiempirical model of large-scale magnetospheric electric fields, *J. Geophys. Res.*, *78*, 171, doi:10.1029/JA078i001p00171.

Wolf, R. A. (1995), Magnetospheric configuration, in *Introduction to Space Physics*, edited by M. G. Kivelson and C. T. Russell, pp. 288–329, Cambridge Univ. Press, Cambridge, U. K.

S. A. Boardsen, Goddard Earth Sciences and Technology Center, University of Maryland Baltimore County, Catonsville, MD 21228, USA.

P. M. E. Décréau and X. Vallières, Laboratoire de Physique et Chimie de l'Environnement et de l'Espace, CNRS, 3A ave. de la rechercher scientifique, F-45071 Orléans CEDEX 02, France.

F. El-Lemdani-Mazouz, Laboratoire Atmosphère, Milieux, Observation Spatiales, CNRS, 11 Boul. D'Alembert, Guyancourt F-78280, France.

C. Foullon, Centre for Fusion, Space and Astrophysics, Department of Physics, University of Warwick, Coventry CV4 7AL, UK.

S. Grimald, Institut de Recherche en Astrophysique et Planétologie, Université Paul Sabatier, CNRS, Toulouse F-31000, France. (grimald@cesr.fr)